Convective Elements in the Marine Atmospheric Boundary Layer. Part I: Conditional Sampling Statistics

GARY K. GREENHUT

Environmental Sciences Group, Environmental Research Laboratories, NOAA, Boulder, CO 80303

SIRI JODHA SINGH KHALSA

Cooperative Institute for Research in Environmental Sciences, University of Colorado/NOAA, Boulder, CO 80309

(Manuscript received 6 September 1986, in final form 14 January 1987)

ABSTRACT

The properties of updrafts and downdrafts through the entire depth of the marine atmospheric boundary layer are investigated using conditional sampling based on an indicator function derived from the vertical velocity time series. Statistics on event size, number density and area occupied are obtained, along with conditional averages of the meteorological variables and percent contributions to the fluxes by updrafts, downdrafts and the environment. A single profile is obtained for convective mass flux based on conditional averaging of updrafts and downdrafts applicable to the fluxes of latent and sensible heat and momentum.

1. Introduction

Discrete parcels of air are known to play a major role in vertical transport within the atmospheric boundary layer. Early descriptions of the boundary layer in which the upward mass flux in plumes is compensated for by overall subsidence of the environment have been modified by including well-defined, downward-moving elements that carry large perturbations in temperature, moisture and horizontal momentum. The existence of discrete downdrafts has been confirmed in images of the convective boundary layer obtained using lidar (Melfi et al., 1985), sodar (Taconet and Weill, 1983) and FM-CW radar (Rowland and Arnold, 1975).

The properties of updrafts and downdrafts in the lower third of the mixed layer have been investigated in papers by Greenhut and Khalsa (1982) and Khalsa and Greenhut (1985) (hereafter referred to as GK and KG, respectively), using the technique of conditional sampling based on an indicator function derived from the time series of vertical velocity perturbations. The present paper extends these results through the entire depth of the marine atmospheric boundary layer. The data analyzed here were obtained on 5 days during the summer of 1984 in a series of flights over the tropical Pacific Ocean. These flights are referred to as the Christmas Island Experiment since a majority of them was based at that location (2°N, 158°W).

The temperature and humidity profiles were similar on all 5 days. Composite profiles of virtual potential temperature (θ_v) and specific humidity (q) are shown in Fig. 1. Wind speed profiles for the 5 days were clearly separated into two categories. The 2 days making up case a in Fig. 1 had rather large shear beginning at the capping inversion located at $z = z_i$. The remaining 3 days forming case b had almost no shear from $0.1z_i$ to $1.5z_i$. The effect of these two rather different wind speed profiles on the conditionally sampled statistics involving horizontal wind perturbations in the upper third of the mixed layer will be interpreted with the aid of a parcel displacement model. The data from the two days in case a are used in a separate companion investigation of entrainment processes at the capping inversion (Khalsa and Greenhut, 1987, hereafter referred to as KG87).

2. Data and scaling parameters

The Christmas Island Experiment occurred during May and June 1984, over the central Pacific Ocean along longitude 150°W between 10°N and 12°S. The latitudes at which aircraft data were obtained for the 5 days used in this analysis are given in Table 1, along with the surface fluxes and scaling parameters. For each day, the flights occurred near the NOAA ship *Researcher* from which simultaneous surface measurements were made and balloon sondes were launched. The flights on days 141 and 151 were at night. No distinction is made between these and the remaining daytime flights in the present analysis.

Turbulence data were obtained using the NOAA gust probe system mounted aboard a NOAA WP-3D research aircraft (Greenhut and Gilmer, 1985). The data were digitized at 80 Hz after low-pass filtering with a four-pole Butterworth filter having a −3 dB point at

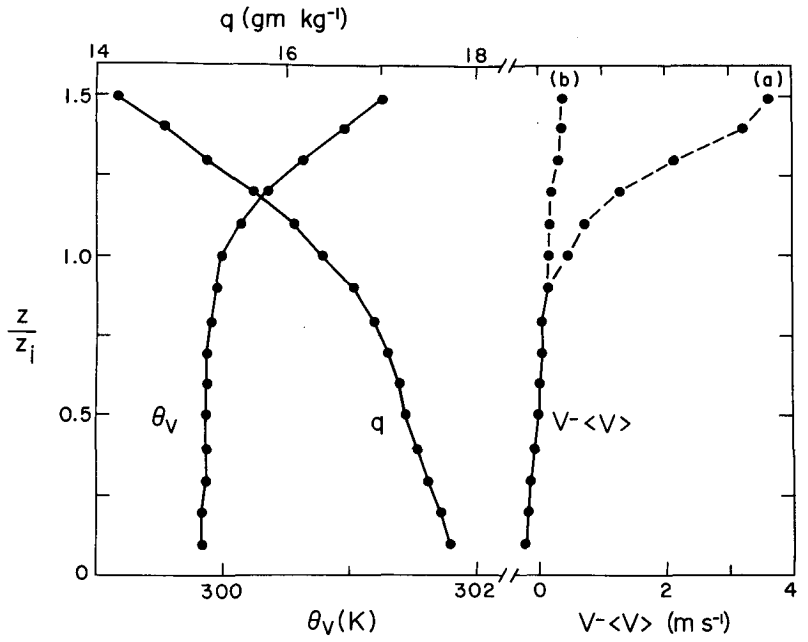

FIG. 1. Composite profiles of virtual potential temperature θ_v, specific humidity q and wind speed deviation $(V - \langle V \rangle)$, where $\langle V \rangle$ is the mean wind speed in the layer $0.1z_i \leq z \leq z_i$ and z_i is the inversion height. Above $0.9z_i$, the wind speed profile is separated into profiles from two sets of days: a) 146 and 151; b) 141, 149 and 154. The profiles are obtained from data taken during aircraft descents and ascents.

11.5 Hz. The mean and linear trend were removed from the time series for each variable during processing, and the sampling rate was reduced to 40 Hz. Fluxes were calculated using the eddy correlation method applied to intervals approximately 5 min (33 km) long.

The heights of the capping inversion z_i, given in Table 1, were determined from profiles of virtual potential temperature θ_v and specific humidity q obtained from aircraft descents and ascents and, to a lesser extent, from balloon sonde launches from the *Researcher*. The composite profiles in Fig. 1, obtained from the aircraft data, show that the layer below z_i was well mixed in terms of virtual potential temperature. Superadiabatic layers just above the surface were frequently observed in the temperature data from the balloon sonde launches (e.g., see Fig. 1 in KG87), but were not observed in the data obtained from the aircraft, which flew as low as 30 m during the daytime flights and 90 m at night. The profiles in Fig. 1 indicate that the layer below the inversion was relatively well mixed with respect to wind speed but not with respect to moisture, becoming steadily drier with height.

The wind profiles in Fig. 1 are relative to the mean wind speed in the layer $0.1z_i \leq z \leq z_i$. From an examination of the wind speed profiles for the 5 days, it was clear that they formed two distinct classes: one with large speed shear above the inversion (case a, consisting of days 146 and 151) and one without speed shear (case b, consisting of days 141, 149 and 154). The composite profiles for the two cases, shown in Fig. 1, overlap below $0.9z_i$ and have been averaged together at those heights. The mean wind speeds in the mixed layer, $\langle V \rangle$, are 4.8 and 9.4 m s^{-1} for cases a and b, respectively. Directional shear was less than 10° within the mixed layer on all 5 days.

For the daytime flights (days 146, 149 and 154), the surface fluxes given in Table 1 were obtained as averages of the fluxes in runs flown at the lowest level, 30

TABLE 1. Inversion height (z_i), surface fluxes of latent heat (E_0), sensible heat (H_0), buoyancy (B_0), and momentum (τ_0), and scaling parameters for the 5 days of the Christmas Island Experiment. All flights took place in the vicinity of 150°W longitude. The scaling parameters were calculated from Eqs. (1)–(5).

Julian day	Latitude	z_i (m)	E_0 (W m^{-2})	H_0 (W m^{-2})	B_0 (W m^{-2})	τ_0 (N m^{-2})	u_* (m s^{-1})	w_* (m s^{-1})	q_* ($\times 10^3$)	T_* (10^{-2} K)	T_{v_*} (10^{-2} K)	$z_i/-L$
141	10°N	500	210	6.2	21.8	0.170	0.38	0.67	0.110	0.78	2.74	2
146	0°	550	80	4.6	10.6	0.037	0.18	0.55	0.052	0.71	1.64	12
149	5°S	450	108	2.9	11.0	0.058	0.22	0.52	0.074	0.47	1.80	5
151	5°S	600	121	6.0	15.1	0.029	0.16	0.63	0.068	0.80	2.02	26
154	12°S	600	143	3.0	13.8	0.068	0.24	0.61	0.083	0.41	1.90	7

m above the surface. For the night flights, the lowest level was at 90 m and, in this case, the surface fluxes were obtained by linear extrapolation of the observed flux profiles to $z = 0$. The scaling parameters in Table 1 were calculated from the standard formulas

$$u_* = (\tau_0/\rho)^{1/2} = [-(\overline{w'u'})_0]^{1/2} \quad (1)$$

$$w_* = \left(\frac{gz_iB_0}{\rho c_pT_0}\right)^{1/3} = \left[\frac{gz_i(\overline{w'T_v'})_0}{T_0}\right]^{1/3} \quad (2)$$

$$q_* = \frac{E_0}{\rho L_v w_*} = \frac{(\overline{w'q'})_0}{w_*} \quad (3)$$

$$T_* = \frac{H_0}{\rho c_p w_*} = \frac{(\overline{w'T'})_0}{w_*} \quad (4)$$

$$T_{v_*} = \frac{B_0}{\rho c_p w_*} = \frac{(\overline{w'T_v'})_0}{w_*}. \quad (5)$$

The subscript 0 denotes the surface value, and g is the gravitational acceleration. Primed quantities are fluctuations about the mean of a run after a linear trend has been removed. In Table 1, the ratios $z_i/-L$, where L is the Monin-Obukhov length, lie between 2 and 26, indicating unstable conditions typical of the tropical marine atmospheric boundary layer.

Composite normalized flux profiles for the 5 days are shown in Fig. 2. The points in these and all subsequent composite profiles were obtained by first averaging all flight legs at a given height on a given day. These averages were then normalized using the scaling parameters in Table 1. All flight days were then combined by averaging within selected height intervals. The number of days contributing at each height in the composite profiles varies from 3 at the lowest level ($0.07z_i$) to a maximum of 6 at $0.67z_i$. As in GK and KG, we find that normalizing the results using mixed-layer scaling parameters causes them to overlap rather well at each normalized height. This is seen in the small error bars in Fig. 2. The obvious exception is the large difference between cases a and b for momentum flux in the upper part of the mixed layer. This represents a breakdown in mixed-layer scaling when shear-driven entrainment effects are strong. In subsequent figures, error bars will not be shown, since they are generally as small as those in Fig. 2.

The flux profiles in Fig. 2 are similar to those obtained previously over tropical oceans (Nicholls and LeMone, 1980; Greenhut and Bean, 1981). The sensible heat flux ($\overline{w'T'}$) changes sign at about $0.35z_i$. This is somewhat higher than typical levels in the data analyzed by KG and may be the result of larger sea–air temperature differences in the present dataset. The profile of buoyancy flux ($\overline{w'T_v'}$) is approximately linear, with an extrapolated value of 0 at $z = z_i$. (When only days 146 and 151 are included in the profile, as in Fig. 4 of KG87, the normalized extrapolated value at $z = z_i$ is −0.16.) In the composite of the 5 days described in this paper, the buoyancy flux at $0.9z_i$ is positive. This is mainly due to the presence of updrafts that remain positively buoyant up to this level. The momentum flux profiles clearly show the effect of strong wind shear above the inversion (case a). A combination of downward entrainment of air with relatively large horizontal wind speed and upward movement of air with relatively low wind speed into the sheared entrainment zone results in large momentum fluxes at $0.9z_i$ (KG87). The contributions of updrafts and

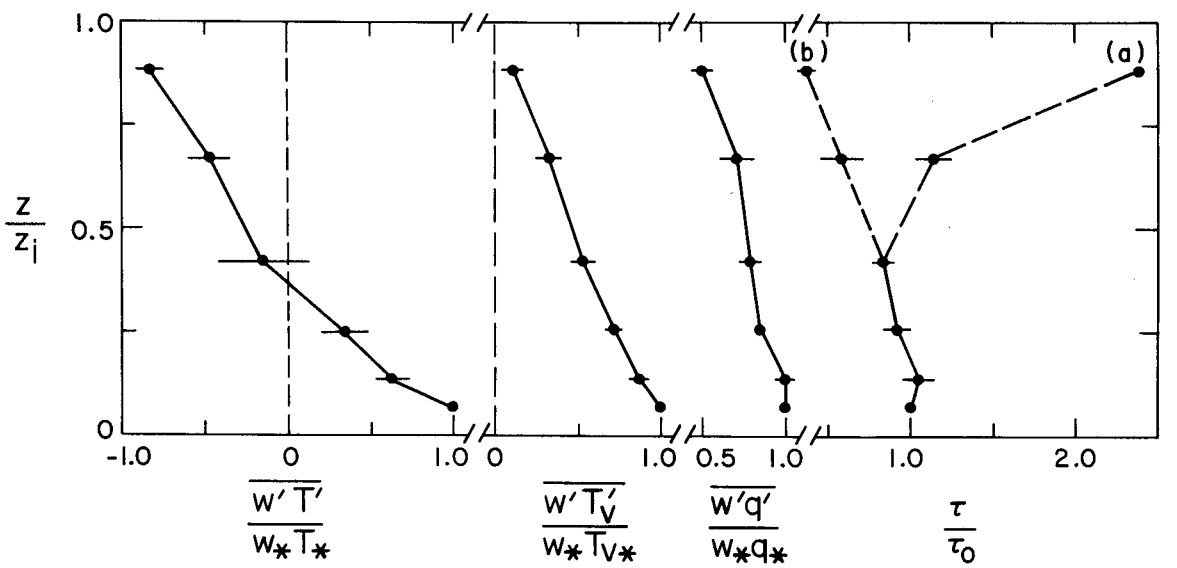

FIG. 2. Composite normalized profiles of the fluxes of temperature ($\overline{w'T'}$), virtual temperature ($\overline{w'T_v'}$), moisture ($\overline{w'q'}$) and momentum (τ). For momentum, cases a and b correspond to those in Fig. 1. The bars indicate the standard errors of the mean.

downdrafts to the flux profiles in Fig. 2 will be discussed in detail in sections 4 and 5.

3. Selection criteria for conditional sampling

The dominant flux-producing events in the atmospheric boundary layer are those associated with updrafts and downdrafts as defined by the time series of vertical velocity (w'). As discussed by GK and KG, the product of the event averages of vertical velocity and another variable, summed over all events, gives approximately 70–80% of the total flux of the variable calculated using the eddy correlation method. In the present paper we continue to use vertical velocity to define updraft and downdraft events. The procedure is described by GK and KG, and the reader is referred to those papers for details. References to previous work on conditional sampling are given by KG. Recently, Godowitch (1986) used our technique to obtain vertical velocity turbulence statistics for boundary layers over urban and rural areas.

As in GK and KG, the threshold for updrafts (downdrafts), w_{th}^{+} (w_{th}^{-}) was set equal to the square root of one-half the variance of all positive (negative) values of w' about $w' = 0$. As shown by GK, this choice of thresholds corresponds to zero average vertical velocity in the environment, defined as that portion of the time series that is neither an updraft nor a downdraft, and this is confirmed in the present dataset. The thresholds were determined separately for each run at each flight level.

An updraft (downdraft) event occurs when w' is larger (smaller) than w_{th}^{+} (w_{th}^{-}) for a minimum time, t_{min}. The use of a minimum event time eliminates small spurious events and prevents large events from being divided by small breaks. In the present analysis, t_{min} has been set equal to 0.2 s corresponding to a minimum event length of 22 m, which is well below the dominant scales of flux-producing events (Mahrt and Paumier, 1984). The minimum event time of 0.2 s corresponds to eight points at a sampling rate of 40 Hz.

During the time that an updraft (downdraft) is present, an indicator function, $I(t)$, is set equal to +1 (−1). Otherwise, it is set equal to 0 (the environment). The indicator function is used to perform conditional sampling on the other variables. In practice, three indicator functions are used: $I^{+}(t)$, $I^{-}(t)$, $I^{0}(t)$, which are +1 during updrafts, downdrafts and the environment, respectively, and 0 otherwise.

To eliminate large-scale variations in the w' time series that would make $I(t)$ unrepresentative of the updrafts and downdrafts at the scales of interest, a high-pass filter having a −3 dB point at 0.014 Hz, has been applied to all time series. This eliminates scales larger than approximately 8 km.

4. Properties of updrafts and downdrafts and their contributions to the total fluxes

a. Size and frequency of events

Profiles of normalized average event size (d/z_i), and normalized number of events per unit length (Nz_i), defined by GK and KG, are shown in Fig. 3 for updrafts, downdrafts and the environment. Also shown are profiles of the product of dN, which is the proportion of the time series occupied by each type of event and which is equal to the area occupied by the events if they are assumed to be randomly distributed (Zipser and LeMone, 1980). There is good agreement between these profiles and those obtained by KG using data up to $\sim 0.3z_i$ over the equatorial Pacific Ocean, except at the lowest level where the present data contain a larger number of events of somewhat smaller size. This is probably due to the fact that we are using a minimum event length of 22 m in the present analysis compared with a corresponding length of 41 m used by KG. The smaller minimum event length allows for smaller events to be included in the statistics, and this will occur most often at the lowest levels where smaller events are most prevalent.

The average normalized sizes of updrafts and downdrafts are approximately equal throughout the mixed layer, increasing from about 0.09 at the lowest level

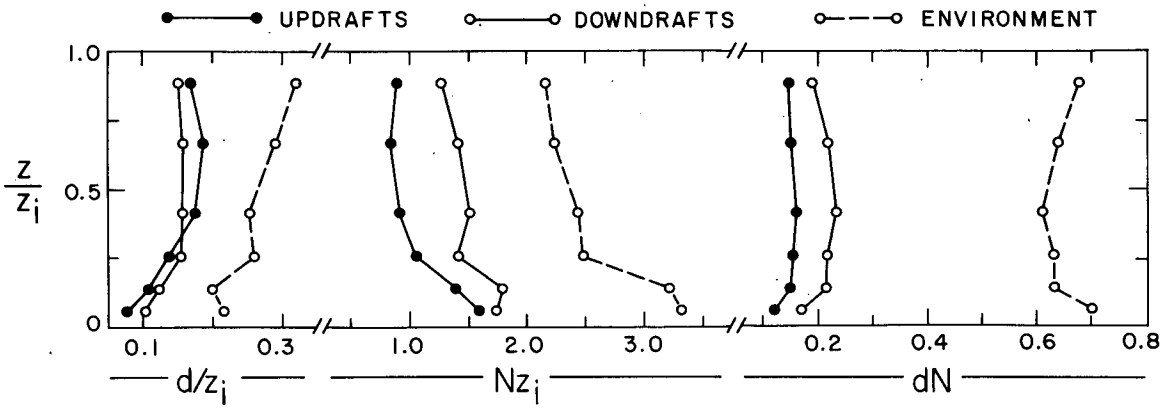

FIG. 3. Profiles of normalized event size (d/z_i), normalized number of events per unit length (Nz_i) and fractional area occupied by events (dN) for updrafts, downdrafts and the environment.

$(0.07z_i)$ to about 0.17 at a height of about $0.3z_i$ and then remaining approximately constant above (Fig. 3). The distance between events (event size of the environment) is approximately twice the size of the events at all heights. Profiles of event size and density are displayed in Fig. 4 using logarithmic scales. Average event size is seen to increase with $(z/z_i)^{1/3}$ up to about $0.4z_i$, in agreement with the observations of Lenschow and Stephens (1980). Also in agreement is the decrease with height of Nz_i with $(z/z_i)^{-1/3}$ for updrafts up to $0.6z_i$.

The number of downdrafts per unit length exceeds that for updrafts at all heights. The number of environmental events per unit length (Fig. 3) is approximately equal to the sum $N^+ + N^-$, since almost all updraft/downdraft events are separated by an event in the environment.

The profiles of area occupied by updrafts and downdrafts (dN) in Fig. 3 are constant with height, approximately 16 and 22%, respectively, except at the lowest and highest levels. At all levels, the area occupied by downdrafts is about 40% larger than the area occupied by updrafts, in approximate agreement with the results obtained by KG up to $0.3z_i$. This is directly related to our choice of thresholds, which ensures that the mean vertical velocity in the environment is zero (Fig. 5), and therefore $d^+N^+w^+ = d^-N^-w^-$, and also to the fact that the vertical velocity frequency distribution is positively skewed (i.e., that updrafts are more vigorous than downdrafts). The ratio $|w^+/w^-|$ is ~ 1.4 when averaged over all heights.

b. Conditional averages

The conditional averages in Fig. 5 are given by

$$x^i = \int_0^{t_{\text{tot}}} x'(t)I^i(t)dt \Big/ \int_0^{t_{\text{tot}}} I^i(t)dt \qquad (6)$$

where t_{tot} is the total time of the sample and $I^i(t)$ ($i = +, -, 0$) and the indicator functions for updrafts, downdrafts and the environment, respectively. The conditional averages are in good agreement with those obtained by KG up to $0.3z_i$. Conditional averages in the environment are small for all the variables.

The presence of large gradients in temperature, moisture and wind speed near the surface, in the entrainment zone and above the inversion produces large values of conditionally averaged specific humidity q and temperature T for updrafts, and also of along-wind momentum u for both updrafts and downdrafts (case a, in particular). The gradients of temperature, moisture and wind speed (case a) near the inversion are evident in the profiles in Fig. 1, which are based on data taken during aircraft descents and ascents. Substantial temperature and moisture gradients were observed near the surface in data obtained from balloon sonde launches from the *Researcher*. The gradients at both the top and bottom of the boundary layer affect the conditional averages at distances well away from the gradient layers because of the transport of surpluses and deficits into the boundary layer by parcel displacement.

The profiles of temperature and moisture perturbations for updrafts in Fig. 5 behave as expected based on the mean profiles of virtual potential temperature and specific humidity shown in Fig. 1. Parcels rising from the superadiabatic layer at the surface remain warm relative to the environment until they reach the level at which their potential temperature is equal to the ambient value. On average, this occurs at about $0.3z_i$ (Fig. 5), which is also the level at which the sensible heat flux changes sign (Fig. 2). Near the top of the mixed layer, updrafts are cool relative to the temperatures in the entrainment zone. Similar considerations apply to the moisture profile for updrafts in Fig. 5. Since the specific humidity profile in Fig. 1 has negative slope throughout the boundary layer and above the inversion, updrafts are predominantly moist relative to the environment at all levels. In Fig. 6, it can be seen that updrafts make the major contribution to all the fluxes at all levels, the contribution by updrafts being two–three times larger than that by downdrafts or the environment. The total flux profiles in Fig. 2 are therefore strongly influenced by the updraft conditional averages in Fig. 5.

The temperature and moisture profiles for downdrafts in Fig. 5 are not symmetrical with respect to those of updrafts since the magnitudes for downdrafts are generally smaller than for updrafts at all levels. The reasons for this will be discussed in detail in section 5 where updrafts and downdrafts are classified according to their thermodynamic properties.

The conditional averages of along-wind momentum u for both updrafts and downdrafts at the lowest level in Fig. 5 are relatively large, due to the presence of a gradient in mean wind speed in the layer below the lowest level sampled by the aircraft. The magnitude of the wind speed perturbations for downdrafts is smaller than that for updrafts at all levels.

There is a strong contrast in the wind speed perturbations for both updrafts and downdrafts at the top of the mixed layer between cases a and b (Fig. 5). In case a, with large wind shear above about $0.9z_i$, downdrafts displaced into the entrainment zone from above arrive with a large horizontal wind speed surplus. The thickness of the entrainment zone can be estimated using $\Delta h \sim w(\omega_B)^{-1}$ (Caughey, 1982), where w is a typical vertical velocity perturbation at the top of the boundary layer (~ 0.5 m s^{-1}) and ω_B is the Brunt–Väisällä frequency

$$\omega_B = \left(\frac{g}{\theta_v}\frac{\partial\theta_v}{\partial z}\right)^{1/2}.$$

Near the inversion, $\theta_v \sim 300$ K and $\partial\theta_v/\partial z \sim 0.002$ K m^{-1} (Fig. 1); therefore $\Delta h \sim 60$ m, which is approximately $0.1z_i$ for the values of z_i in Table 1. The large negative wind speed perturbation for updrafts at $0.9z_i$ in Fig. 5 (case a) indicates that the large wind

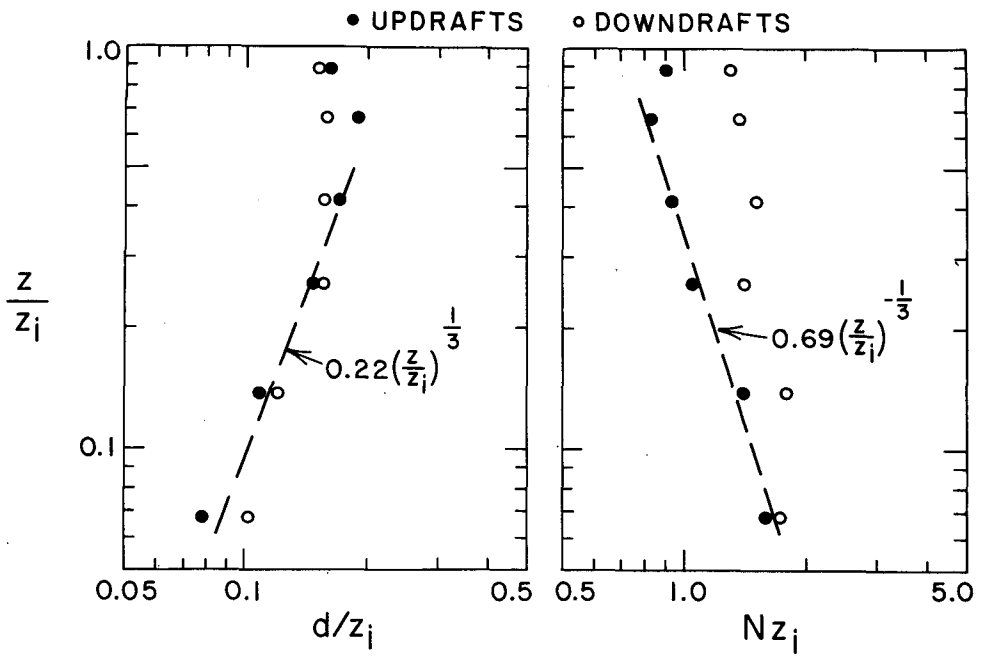

FIG. 4. Profiles of d/z_i and Nz_i, as in Fig. 3, but plotted on logarithmic scales.

shear has an effect at least $0.1z_i$ below the bottom of the wind shear layer.

c. *Event contributions to the fluxes*

The relative contributions to the total fluxes, normalized by the surface fluxes for updrafts, downdrafts and the environment are shown in Fig. 6. Updrafts make the largest contributions at all levels, the ratios being approximately 55%:25%:20% at a majority of the levels for updrafts, downdrafts and the environment, respectively, in good agreement with the observations of KG. The environment makes its largest contribution

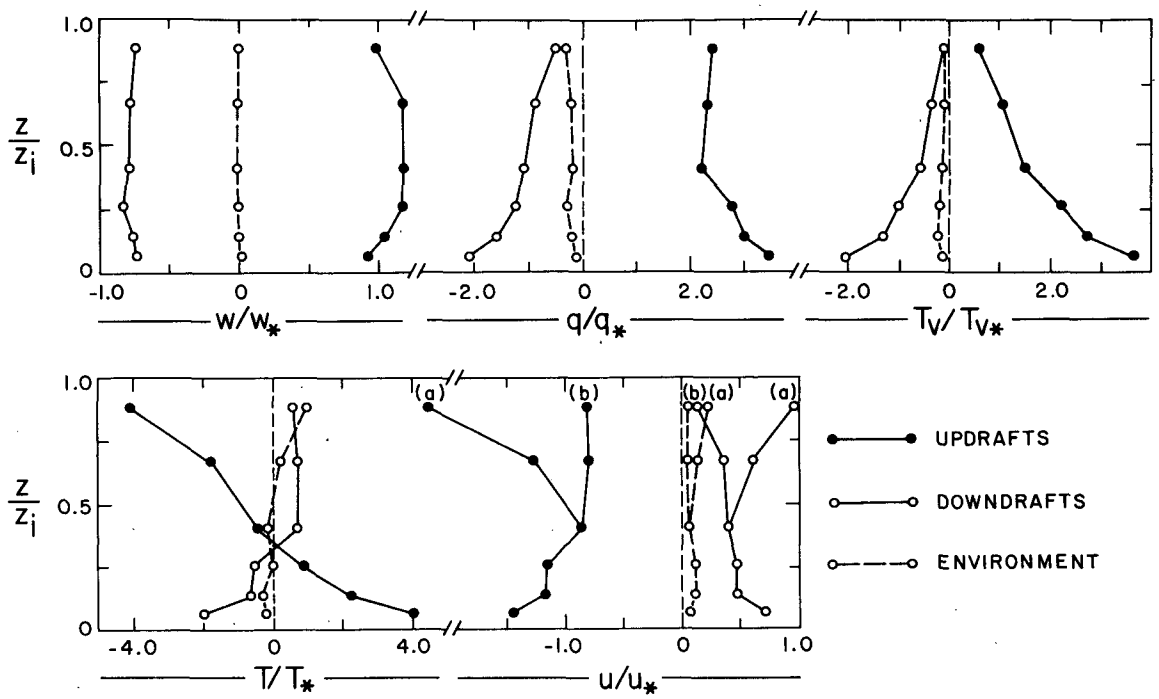

FIG. 5. Profiles of normalized conditional averages of vertical velocity w, specific humidity q, virtual temperature T_v, temperature T and along-wind momentum u for updrafts, downdrafts and the environment. For u, the two profiles correspond to cases a and b in Fig. 1.

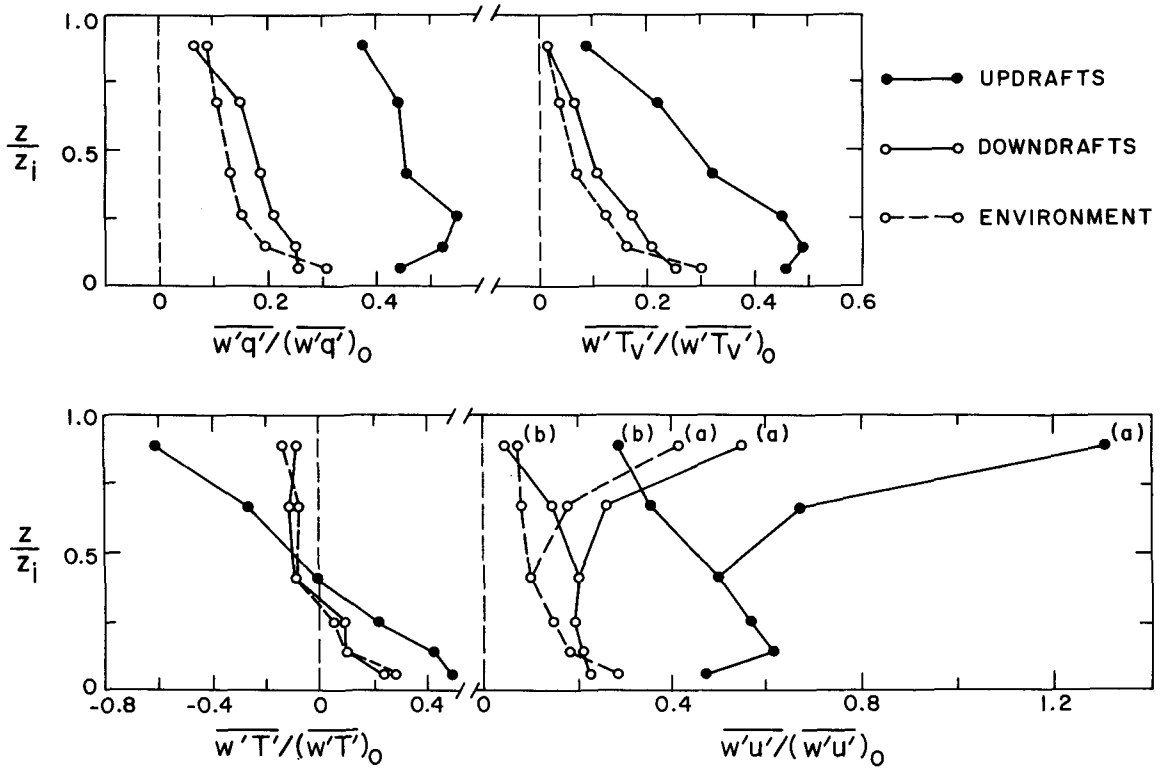

FIG. 6. Profiles of the relative contribution to the total fluxes of latent heat ($\overline{w'q'}$), buoyancy ($\overline{w'T_v'}$), sensible heat ($\overline{w'T'}$) and along-wind momentum ($\overline{w'u'}$) normalized by the surface fluxes, for updrafts, downdrafts and the environment.

to the fluxes at the lowest level ($0.07z_i$), exceeding the contribution made by downdrafts.

It was found by KG that the contribution to the flux of x by updrafts and downdrafts is well approximated by the product of the mean vertical velocity and mean value of x within the events, weighted by the proportion of the area occupied:

$$F_x^{\pm} \approx d^{\pm}N^{\pm}\frac{w^{\pm}}{w_*}\frac{x^{\pm}}{x_*} \tag{7}$$

where $F_x^{\pm}$ is the normalized flux of x. We compared the latent heat and buoyancy fluxes calculated using (7) with the total normalized fluxes in Fig. 6. In both cases, we find that for updrafts, (7) underestimates the fluxes at all levels by approximately 10% and for downdrafts, (7) overestimates the fluxes by about 5%. The small-scale correlated fluctuations within updraft events contribute 10% of the flux produced by updrafts (i.e., ~6% of the total flux at most levels). The small-scale fluctuations within downdraft events are correlated in an opposite sense to the correlation of the larger flux-producing scales and make a negative contribution (~ −5%) to the flux produced by downdrafts (~ −1% of the total flux at most levels).

Since the mean values of w and x averaged over all environmental events are very small (Fig. 5), (7) cannot be used to estimate the contribution of the environment to the total flux. The environmental contribution can be separated into two parts: a "bulk contribution" equal to the sum over all environmental events of $\bar{w}\bar{x}$, representing large-scale correlations, and the residual, which comes from correlated small-scale fluctuations within each environmental event. The bulk contribution is routinely calculated when the time series are conditionally sampled. We find that the small-scale fluctuations contribute about 75% of the flux due to the environment at the lowest level of observation ($0.07z_i$), decreasing to about 50% in the middle and upper levels of the mixed layer. Thus, the large environmental contributions to the fluxes at the lowest level in Fig. 6 are due, in part, to the presence of a large number of small-scale fluctuations that are not selected as updrafts or downdrafts due to the minimum event length criterion.

5. Thermodynamic classification of updrafts and downdrafts

Additional insight is gained into the behavior of updrafts and downdrafts when they are subclassified according to their temperature and moisture characteristics. Following GK and KG, each event was categorized according to whether its temperature perturbation was positive (warm) or negative (cool), and whether its specific humidity perturbation was positive (moist) or negative (dry). Statistics and conditional averages were then obtained within the four resulting subclassifications. Results are shown in Fig. 7 for fractional area occupied (dN) and for the conditional averages of

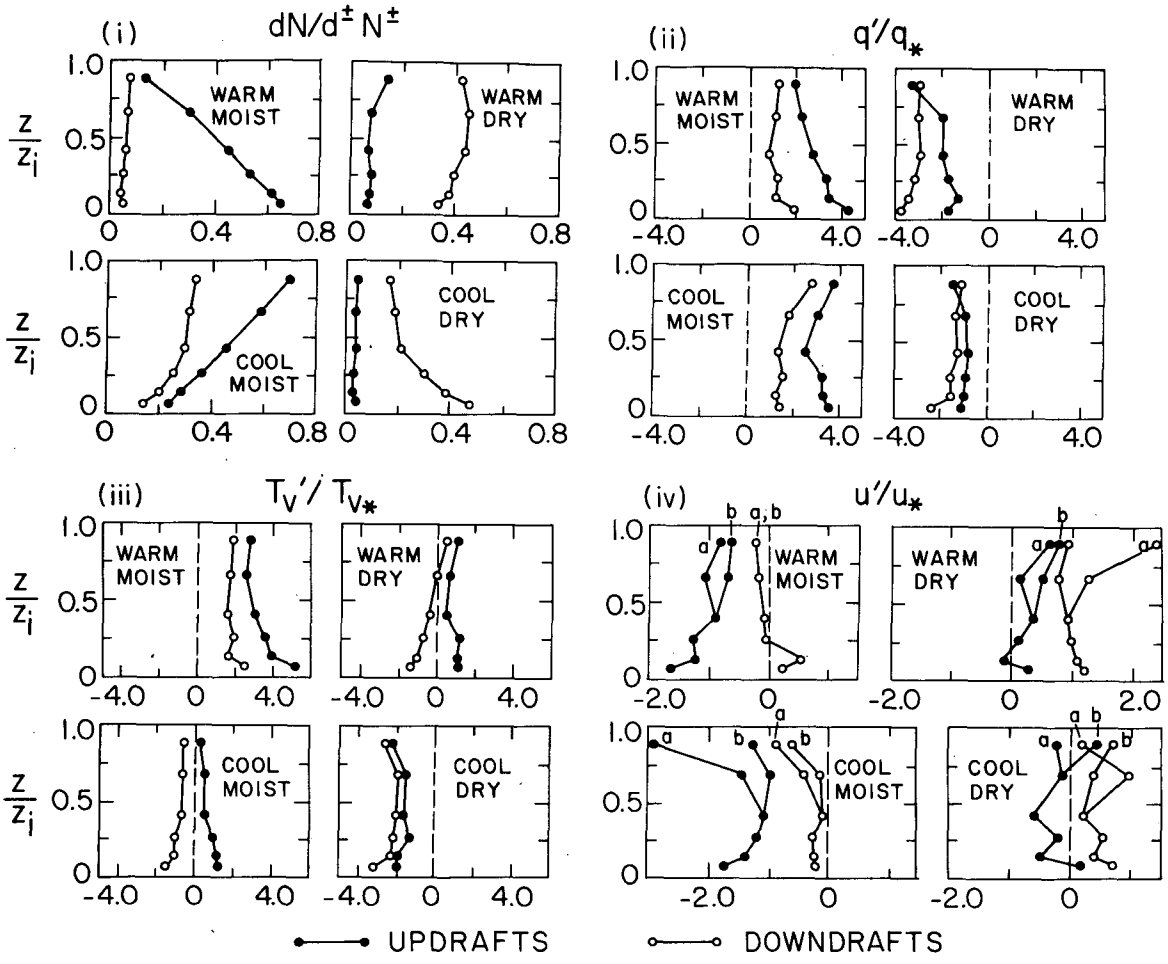

FIG. 7. Profiles of (i) fractional area occupied (dN) normalized by the total fractional area occupied by updrafts or downdrafts at the corresponding height (Fig. 3), and normalized conditional averages of (ii) specific humidity, (iii) virtual temperature and (iv) along-wind momentum for updrafts and downdrafts subclassified by temperature and moisture content.

moisture, virtual temperature and along-wind momentum.

The major classes of events are those with the larger values of dN in the four panels in Fig. 7(i), namely, warm and cool moist updrafts and warm and cool dry downdrafts. The remaining minor classes—dry updrafts and moist downdrafts—occupy a small area with the exception of cool/moist downdrafts. The minor classes arise mainly from overturning. Evidence for this is the fact that, in general, the minor events have the same sign of u' as the events prior to overturning. For example, minor downdrafts have negative u', indicating that their origin is from below the level of observation; the opposite is true for minor updrafts. (Cool/dry updrafts are an exception at intermediate levels, but there are very few such events and the u' statistics probably contain a large uncertainty in this case.)

The asymmetry of the profiles of temperature and moisture perturbations between updrafts and downdrafts in Fig. 5 can be understood in terms of the fractional area occupied by the subclassified events in Fig. 7(i). The observed increase (decrease) with height in area occupied by cool (warm)/moist updrafts occurs because upward-moving parcels rising from a moist, superadiabatic layer move through levels that are increasingly drier and through a height at which the ambient potential temperature is equal to and then exceeds the potential temperature of the parcel. The profiles of area occupied by cool/dry downdrafts and warm/moist updrafts in Fig. 7(i) behave similarly with height. The area occupied by cool/dry downdrafts increases with decreasing height as the downdrafts enter the region of influence of the superadiabatic layer below. The area occupied by warm/dry and cool/moist downdrafts do not behave in a way that is analogous to their counterparts, cool/moist and warm/dry updrafts, respectively. Instead of a decrease in area occupied with decreasing height, warm/dry downdrafts occupy a large area almost to the lowest level of observation. Similarly, cool/moist downdrafts occupy a substantial area for a minor class of events (compared with warm/dry updrafts). This is presumably due to the fact that cool/moist downdrafts acquire negative buoyancy after cool/moist updrafts have overturned [see Fig. 7(iii)]. The

small value of negative temperature perturbation near the surface for downdrafts taken as a whole (Fig. 5) is now explained by the large area occupied by warm/dry downdrafts near the surface; the small value of positive temperature perturbation for downdrafts near the top of the boundary layer is due to the large area occupied by cool/moist downdrafts at that level. Similarly, the large area occupied by cool/moist downdrafts near the top causes the negative moisture perturbation at that level for downdrafts to be small (Fig. 5).

6. Convective mass flux parameterization

A parameterization, originally developed by Betts (1975) to describe vertical fluxes in clouds, was later extended to describe convection in the subcloud layer (Betts, 1976) and used to interpret flux profiles derived from budget studies (Esbensen, 1975). Nicholls and LeMone (1980) used this parameterization to derive a profile of convective mass flux in the subcloud layer based on data obtained over the tropical Atlantic Ocean during the GARP Atlantic Tropical Experiment (GATE). The parameterization represents the flux of a quantity x as the product of the convective mass flux and the difference $x_c - \bar{x}$, where x_c is the value of x inside convective elements and $\bar{x}$ is the average over a flight leg. This parameterization was extended by KG to subcloud updrafts and downdrafts:

$$\overline{w'x'} = \omega_x^*(x^+ - x^-) \tag{8}$$

where ω_x^* is the convective mass flux associated with the quantity x, and $x^+(x^-)$ is the conditionally averaged value of x for updrafts (downdrafts). (The notation for the parameter ω_x^* was ω_x^{**} in KG.) More recently, Penc and Albrecht (1986) made an analysis similar to that of KG using data from STRATEX (Marine Stratus Experiment), where their updrafts are defined in the same way as x_c in the case of Nicholls and LeMone; namely, they are defined as that part of the time series having colocated positive values of w' and q', and downdrafts are that part of the time series with colocated negative values of w' and q'.

Using (8) and the data from the Christmas Island Experiment, we derived profiles of ω_x^* for the fluxes of latent and sensible heat and momentum and find that they agree with one another to within a standard error, including separately derived profiles of ω_u^* for cases a and b (Fig. 1). This agreement implies that the single average profile of ω^*/w_* in Fig. 8 is applicable to a wide range of conditions within and above the mixed layer.

The values of ω^*/w_* in Fig. 8 are somewhat smaller than the observations of Betts (1976) and Nicholls and LeMone (1980), which is to be expected since our updraft/downdraft differences are presumably larger than their convective element difference taken relative to the flight mean. Penc and Albrecht (1986) analyze their data using both updraft/downdraft differences and the difference between updrafts and the flight mean and found that, in the latter case, ω^* is larger by 20–50%, depending on height. Our results lie within the variation of normalized mass flux profiles obtained by Penc and Albrecht under varying degrees of boundary-layer mixing, capping inversion strength and cloud cover. However, the large positive slope of the profile in Fig. 8 near the surface is not seen in their profiles. Penc and Albrecht point out that for trade cumulus, mass entrainment near the surface is balanced by detrainment near the top of the mixed layer. In their case of boundary layers topped by stratocumulus clouds, entrainment and detrainment are in balance throughout the subcloud layer.

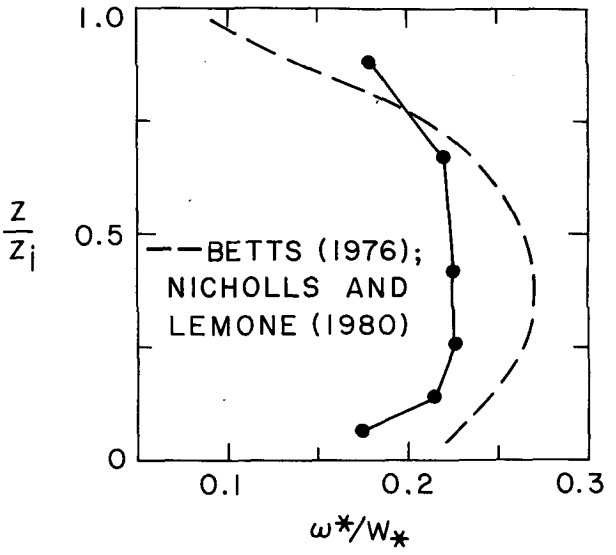

FIG. 8. Profile of normalized convective mass flux derived from Eq. (8) and applicable to the fluxes of latent and sensible heat and momentum. The dashed curve corresponds to the overlapping mass flux profiles obtained by Betts (1976) and Nicholls and LeMone (1980).

7. Summary

Our study of the properties of flux-producing updrafts and downdrafts using data obtained during the Christmas Island Experiment in 1984 extends the results of GK and KG to the entire depth of the marine atmospheric boundary layer. The mean sizes of updrafts and downdrafts d are approximately equal at all heights whereas the number of downdrafts per unit length N, as well as their area occupied, is greater than that for updrafts. The height variation in the lower boundary layer for normalized d and N (updrafts only) is $(z/z_i)^{1/3}$ and $(z/z_i)^{-1/3}$, respectively, in agreement with previous observations of Lenschow and Stephens (1980).

Two of the 5 days in the Christmas Island Experiment had large wind shear above the inversion. On these days, the momentum flux in the entrainment zone at the top of the boundary layer is large, contributed to mainly by cool/moist updrafts entering the zone

of large wind shear and warm/dry downdrafts bringing high momentum air downward. In general, updrafts make the largest contribution to the latent and sensible heat and momentum fluxes at all levels, two–three times as large as the contributions of downdrafts or the environment. The contribution to the fluxes by updrafts and downdrafts comes almost entirely from the mean vertical velocity and transported quantity (T, q or u) within the drafts. The flux contribution from the environment outside of the drafts vary from ~30% near the surface to ~5–10% at $0.9z_i$.

A convective mass flux parameter is derived based on the difference between updraft and downdraft perturbations. A single profile of this parameter is found to be applicable to the fluxes of latent and sensible heat and momentum under a range of conditions within and above the mixed layer.

This analysis of data from the Christmas Island Experiment completes our description of the properties of updrafts and downdrafts in the undisturbed marine atmospheric boundary layer. Future work using the conditional sampling technique will include a study of the effect of varying surface conditions on the structure of boundary layer turbulence using data obtained during FASINEX (Frontal Air–Sea Interaction Experiment) (Stage and Weller, 1985, 1986), studies of cloud–subcloud interactions and the interaction of turbulence and radiation in the stratocumulus-topped boundary layer.

Acknowledgments. This research was supported by the Marine Meteorology Program of the Office of Naval Research under Contracts N00014-84-K-0405 and N00014-86-F-0035.

REFERENCES

Betts, A. K., 1975: Parametric interpretation of trade-wind cumulus budget studies. *J. Atmos. Sci.*, **32,** 1934–1945.

——, 1976: Modeling subcloud layer structure and interaction with a shallow cumulus layer. *J. Atmos. Sci.*, **33,** 2363–2382.

Esbensen, S., 1975: An analysis of subcloud-layer heat and moisture budgets in the western Atlantic trades. *J. Atmos. Sci.*, **32,** 1921–1933.

Caughey, S. J., 1982: Observed characteristics of the atmospheric boundary layer. *Atmospheric Turbulence and Air Pollution Modeling.* (F. T. M. Nieuwstadt and H. van Dop, Eds.), Reidel, 107–158.

Godowitch, J. M., 1986: Characteristics of vertical turbulent velocities in the urban convective boundary layer. *Bound.-Layer Meteor.*, **35,** 387–407.

Greenhut, G. K., and B. R. Bean, 1981: Aircraft measurements of boundary layer turbulence over the central equatorial Pacific Ocean. *Bound.-Layer Meteor.*, **14,** 513–523.

——, and R. O. Gilmer, 1985: Calibration and accuracy of the NOAA/ERL gust probe system and intercomparison with other systems. NOAA Tech. Memo. ERL ESG-22, 30 pp.

——, and S. J. S. Khalsa, 1982: Updraft and downdraft events in the atmospheric boundary layer over the equatorial Pacific Ocean. *J. Atmos. Sci.*, **39,** 1803–1818.

Khalsa, S. J. S., and G. K. Greenhut, 1985: Conditional sampling of updrafts and downdrafts in the marine atmospheric boundary layer. *J. Atmos. Sci.*, **42,** 2550–2562.

——, and ——, 1987: Convective elements in the marine atmospheric boundary layer. Part II: Entrainment at the capping inversion. *J. Climate Appl. Meteor.*, **26,** 824–836.

Lenschow, D. H., and P. L. Stephens, 1980: The role of thermals in the convective boundary layer. *Bound.-Layer Meteor.*, **19,** 509–532.

Mahrt, L., and J. Paumier, 1984: Heat transport in the atmospheric boundary layer. *J. Atmos. Sci.*, **41,** 3061–3075.

Melfi, S. H., J. D. Spinhrine, S.-H. Chou and S. P. Palm, 1985: Lidar observations of vertically organized convection in the planetary boundary layer over the ocean. *J. Climate Appl. Meteor.*, **24,** 832–847.

Nicholls, S., and M. A. LeMone, 1980: The fair weather boundary layer in GATE: The relationship of subcloud fluxes and structure to the distribution and enhancement of cumulus clouds. *J. Atmos. Sci.*, **37,** 2051–2067.

Penc, R. S., and B. A. Albrecht, 1986: Parametric representation of heat and moisture fluxes in cloud-topped mixed layers. *Bound.-Layer Meteor.*, in press.

Rowland, J. R., and A. Arnold, 1975: Vertical velocity structure and geometry of clear air convective elements. *Preprints, 16th Conf. Radar Meteorology,* Houston, Amer. Meteor. Soc., 296–303.

Stage, S. A., and R. A. Weller, 1985: The Frontal Air-Sea Interaction Experiment (FASINEX). Part I: Background and scientific objectives. *Bull. Amer. Meteor. Soc.*, **66,** 1511–1520.

——, and R. A. Weller, 1986: The Frontal Air-Sea Interaction Experiment (FASINEX). Part II: Experimental plan. *Bull. Amer. Meteor. Soc.*, **67,** 16–20.

Taconet, O., and A. Weill, 1983: Convective plumes in the atmospheric boundary layer as observed with an acoustic Doppler sodar. *Bound.-Layer Meteor.*, **25,** 143–158.

Zipser, E. J., and M. A. LeMone, 1980: Cumulonimbus vertical velocity events in GATE. Part II: Synthesis and model core structure. *J. Atmos. Sci.*, **37,** 2458–2469.